NAVAL SHIP RESEARCH AND DEVELOPMENT CENTER
Washington, D. C. 20034

SOUNDS GENERATED BY THE IMPLOSION OF HOLLOW STRUCTURES UNDER HYDROSTATIC PRESSURE

by

George Chertock and Wayne E. Reader

SHIP ACOUSTICS DEPARTMENT

RESEARCH AND DEVELOPMENT REPORT

November 1970

Report 3537

The Naval Ship Research and Development Center is a U.S. Navy center for laboratory effort directed at achieving improved sea and air vehicles. It was formed in March 1967 by merging the David Taylor Model Basin at Carderock, Maryland and the Marine Engineering Laboratory (now Naval Ship R & D Laboratory) at Annapolis, Maryland. The Mine Defense Laboratory (now Naval Ship R & D Laboratory) Panama City, Florida became part of the Center in November 1967.

Naval Ship Research and Development Center
Washington, D. C. 20034

MAJOR NSRDC ORGANIZATIONAL COMPONENTS

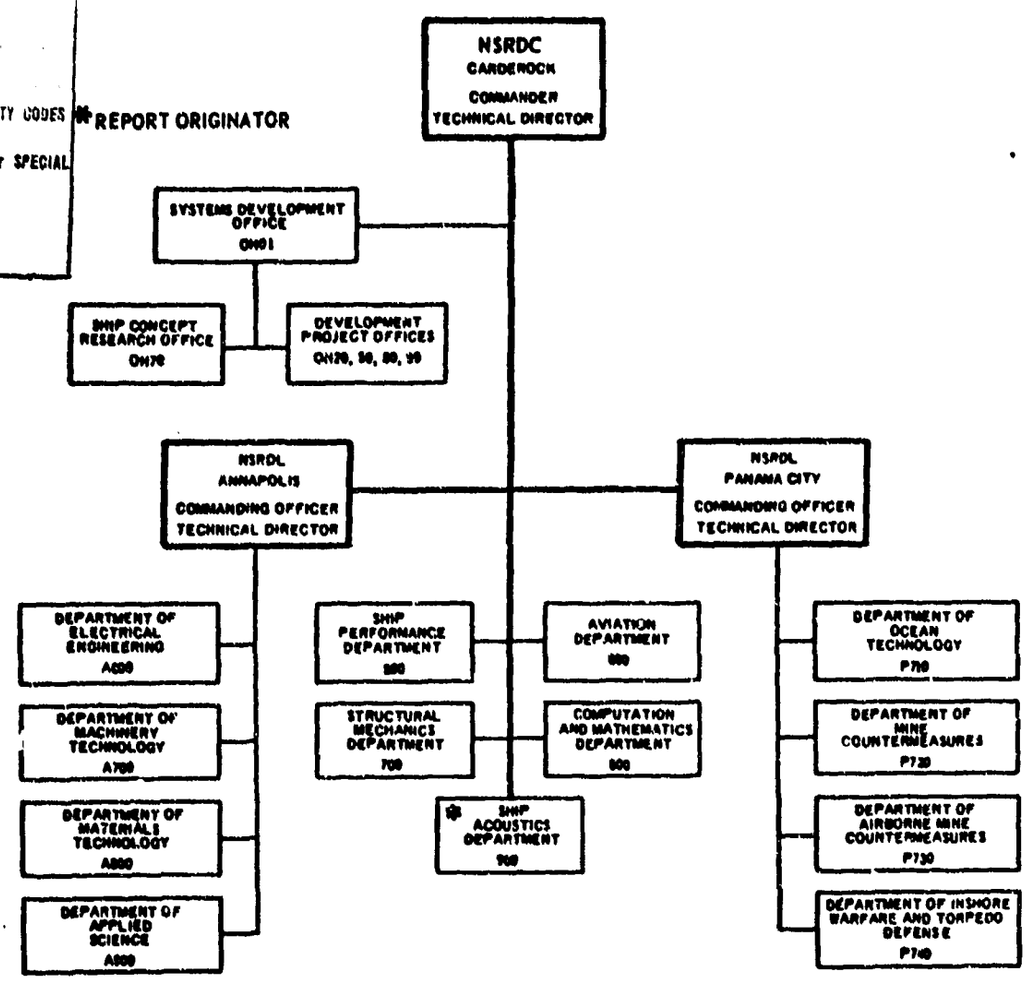

UNCLASSIFIED
Security Classification

DOCUMENT CONTROL DATA - R & D

(Security classification of title, body of abstract and indexing annotation must be entered when the overall report is classified)

1. ORIGINATING ACTIVITY (Corporate author) Naval Ship Research and Development Center Washington, D.C. 20034	2a. REPORT SECURITY CLASSIFICATION UNCLASSIFIED 2b. GROUP 2

3. REPORT TITLE

SOUNDS GENERATED BY THE IMPLOSION OF HOLLOW STRUCTURES UNDER HYDROSTATIC PRESSURE

4. DESCRIPTIVE NOTES (Type of report and inclusive dates)

Interim Report

5. AUTHOR(S) (First name, middle initial, last name)

George Chertock and Wayne T. Reader

6. REPORT DATE	7a. TOTAL NO. OF PAGES	7b. NO. OF REFS
November 1970	47	7

8a. CONTRACT OR GRANT NO. b. PROJECT NO. R01101 c. TASK AREA ZR0110101 d. WORK UNITS 903-008 and 945-051	9a. ORIGINATOR'S REPORT NUMBER(S) 3537 9b. OTHER REPORT NO(S) (Any other numbers that may be assigned this report)

10. DISTRIBUTION STATEMENT

11. SUPPLEMENTARY NOTES	12. SPONSORING MILITARY ACTIVITY
	NAVMAT, Code 03L4

13. ABSTRACT

We analyze the mechanism by which a particular structure implodes under hydrostatic pressure, calculate the accelerated motions of the boundary surface, and calculate the magnitude and distribution of the sounds which are produced. We then describe experiments to verify the theoretical analysis of the motion and the sound generation. The limited and incomplete experimental data which are presently available substantially confirm the theoretical analysis. In particular, the theory and experiments show that the principal component of the transient sound is the same in all directions and is proportional to the second time derivative of the volume enclosed by the wetted surface of the imploding structure. There are some uncertainties in the interpretation of the data, but these should be resolved by the remaining test program.

DD FORM 1 NOV 68 1473 (PAGE 1)

S/N 0101-807-6801

UNCLASSIFIED
Security Classification

14 KEY WORDS	LINK A		LINK B		LINK C	
	ROLE	WT	ROLE	WT	ROLE	WT
IMPLOSION						
RADIATED SOUND PRESSURE						
IMPLODER						
LINEAR ENERGY ABSORBER						
TRANSIENT PRESSURE PULSE						

DEPARTMENT OF THE NAVY
NAVAL SHIP RESEARCH AND DEVELOPMENT CENTER
WASHINGTON, D. C. 20034

SOUNDS GENERATED BY THE IMPLOSION OF HOLLOW STRUCTURES UNDER HYDROSTATIC PRESSURE

by

George Chertock and Wayne T. Reader

November 1970

Report 3537

TABLE OF CONTENTS

LIST OF FIGURES

Page

ABSTRACT

We analyze the mechanism by which a particular structure implodes under hydrostatic pressure, calculate the accelerated motions of the boundary surface, and calculate the magnitude and distribution of the sounds which are produced. We then describe experiments to verify the theoretical analysis of the motion and the sound generation. The limited and incomplete experimental data which are presently available substantially confirm the theoretical analysis. In particular, the theory and experiments show that the principal component of the transient sound is the same in all directions and is proportional to the second time derivative of the volume enclosed by the wetted surface of the imploding structure. There are some uncertainties in the interpretation of the data, but these should be resolved by the remaining test program.

ADMINISTRATIVE INFORMATION

This work was principally performed under the Foundation Research Program of the Naval Ship Research and Development Center, Task Area ZR0110101, Task IR, Work Units 903-008 and 945-051. Portions of the material in this report were also contained in a thesis submitted by W.T. Reader to the Faculty of the School of Engineering and Architecture, Catholic University of America, in partial fulfillment of the requirements for the degree Doctor of Philosophy (May 1970).

INTRODUCTION

Our objective is (1) to explain the magnitude and distribution of the sound which is generated by the implosion of a hollow structure under external pressure in deep water and (2) to verify the theoretical analysis by experiments under controlled conditions.

By an implosion we mean a sudden collapse of the structure which occurs when the external pressure reaches some characteristic critical value and triggers an unstable deformation. The deformation is unstable because the external pressure forces continue to exceed the internal restoring forces generated by the deformation. Eventually the forces balance, the kinetic energy is dissipated, and the motion is arrested.

During the implosion, sound can be generated by a variety of processes such as the inrush of water, the impact of two parts of the structure, or the sudden compression of the trapped air. These processes all generate accelerated motions of the boundary surface of the structure and thus radiate sound into the water.

Despite the great complexity and variability in possible motions of the boundary surface, however, we show that for a wide range of practical cases, the sound pressure in the far field of a uniform medium is the same for all directions and is simply proportional to the second time derivative of the volume enclosed by the wetted surface. Also, we show how the history of this volume acceleration depends on the initial pressure difference and on the internal forces which resist the collapse.

This analysis is confined to predicting the shape of the sound pulse as it is affected by the implosion mechanism and as it would be in a uniform unbounded medium. In any real situation where the pulse propagates over very long ranges in the sea, the initial shape of the pulse

would be enormously distorted by multipaths, by velocity gradients in the water, and by scattering; the pattern of implosion sound at some distant point would be determined principally by the geography of the path.

The experiments are made with a simple imploding structure for which both the collapsing motions and the sound pulse can be predicted theoretically and measured with precision.

The present report is only a progress report because the experimental program has not been completed. However, even the limited experimental data that are available clearly verify the main features of the theoretical analysis. The additional experimental data from the remainder of the program are expected to resolve any uncertainties remaining in the analysis.

THEORETICAL ANALYSIS

THEORY AND ANALYSIS OF THE GENERAL CASE

We start with the Kirchhoff equation[1] for the instantaneous sound pressure $p(\underline{r},t)$ at an arbitrary field point $\underline{r}$ and time t in terms of the prior values of the sound pressure, its time derivative, and its normal gradient at all points $\underline{s}$ on a fixed surface which encloses the imploding body.

$$p(\underline{r},t) = -\iint \left[\frac{\partial p}{\partial n} \right] \frac{d\sigma}{4\pi R} - \iint \frac{[\dot{p}]}{c} \frac{\partial R}{\partial n} \frac{d\sigma}{4\pi R} - \iint \frac{[p]}{R} \frac{\partial R}{\partial n} \frac{d\sigma}{4\pi R} \qquad (1)$$

Here $\underline{n}(\underline{s})$ is a local normal pointing outward, $\underline{R} = \underline{r} - \underline{s}$, and the bracket notation signifies that the term within the brackets is to be evaluated

[1] References are listed on page 43.

for the retarded time $t^*(\underline{s}) = t - R/c$, e.g.,

$$[p(\underline{s},t)] = p(\underline{s},t^*) = p(\underline{s},t - R/c) \tag{2}$$

Thus, the entire sound pressure field is expressed by the history of the sound pressure at the closed surface. However, the form of the relation is inconvenient to analyze (1) because the retarded time at which each integrand is to be evaluated varies from point to point in each integral, (2) because each integrand is a complicated mixed function of the coordinates of the field point $\underline{r}$ as well as the surface point $\underline{s}$, and (3) because the point $\underline{s}$ identifies a geometrical location on a fixed surface rather than a material point on the body for which it would be simpler to write an equation of motion.

Hence, we take the origin at some convenient reference point (to be determined) within the surface and refer all terms in the integrands to a common retarded time $t_o^* = t - r/c$. We do this by expanding each function of the retarded time as a Taylor series about $t^* = t_o^*$. Thus for the function $q(s,t^*) = [\partial p/\partial n]$

$$q(s,t^*) = \sum_n \frac{1}{n!}(t^* - t_o^*)^n \left.\frac{d^n q}{dt^{*n}}\right|_{t^*=t_o^*} \tag{3}$$

and similar series expansions apply to $[p]$ and $[\dot{p}]$. Also we restrict the application of Equation (1) to the far field where r is much larger than the maximum dimension of the closed surface s. Then

$$\frac{1}{R} = \frac{1}{r}\,[1 + O(s/r)] \tag{4}$$

$$t^* - t_o^* = \frac{r - R}{c} = \frac{s}{c} \cos(\underline{s},\underline{r}) \left[1 + O(s/r)\right] \tag{5}$$

Now we substitute Equations (3), (4), and (5) into Equation (1), retain only those terms which are $O(s/r)$, and apply the boundary condition

$$\frac{\partial p}{\partial n} = - \rho v \tag{6}$$

where $v(\underline{s},t)$ is the outward normal velocity at $(\underline{s},t)$. The result is a conventional multipole expansion[2] with contributions from the first two integrals in Equation (1) but with no far-field contribution from the third integral.

$$p(\underline{r},t) = \frac{1}{4\pi r} \left\{ \sum_{m=0}^{\infty} \iint \left[\frac{s \cos(\underline{s},\underline{r})}{c}\right]^m \frac{1}{m!} \frac{d^m(\rho \hat{v})}{dt^m} \, d\sigma \right.$$

$$\left. - \sum_{m=1}^{\infty} \iint \left[\frac{s \cos(\underline{s},\underline{r})}{c}\right]^{m-1} \frac{\cos(\underline{n},\underline{r})}{c(m-1)!} \frac{d^m p}{dt^m} \, d\sigma + \ldots \right\} \tag{7}$$

where all terms are to be evaluated at the common time $t_o^* = t - r/c$. We transform this to a form where all integrals are independent of the position of the field point and, furthermore, where each multipole term has a simple physical interpretation.

$$p(\underline{r},t) = \frac{1}{4\pi r} \left[\iint \rho \hat{v} \, d\sigma \right]$$

$$+ \frac{1}{4\pi r c} \frac{d}{dt} \left[\iint (\rho \hat{v} \underline{s} - p\underline{n}) \, d\sigma \right] \cdot \hat{\underline{r}}$$

$$+ \frac{1}{4\pi r c^2} \hat{\underline{r}} \cdot \frac{d^2}{dt^2} \left[\frac{1}{2} \iint \underline{s}(\rho \hat{v} \underline{s} - 2p\underline{n}) \, d\sigma \right] \cdot \hat{\underline{r}} + \ldots \tag{8}$$

The bracketed factor in the first term is simply $\rho\dot{V}$ where $\rho\dot{V}(t_o^*)$ is the outward flux of water through the closed surface. The sound field is the same in all directions and is the same as that of a simple source (monopole) whose instantaneous source strength is $\dot{V}(t_o^*)$.

The second term is a dipole field $\frac{\dot{F}}{} \cos(\underline{F},\underline{r})/4\pi rc$ which is the same as though a concentrated force $\underline{F}(t_o^*)$ were applied at the origin in an unbounded uniform medium, and where the vector force $\underline{F} = \iint(\rho\dot{\underline{v}}\underline{s} - p\underline{n})d\sigma$. The second term in $\underline{F}$ is simply the unsteady force exerted by the water on the surface; the first term can be interpreted as an inertia force associated with the linear momentum of the surface motion.

The third term in Equation (8) is a quadrupole field $(\hat{\underline{r}}\cdot\ddot{Q}\cdot\hat{\underline{r}})/(4\pi rc^2)$ which is the same as though an equivalent dyadic torque $Q(t_o^*) = \frac{1}{2}\iint \underline{s}(\rho\dot{\underline{v}}\underline{s} - 2p\underline{n})\, d\sigma$ were applied at the origin in an unbounded medium. The second part of Q is simply the unsteady torque exerted by the water on the closed surface; the first part is an inertia moment associated with the angular momentum of the surface motion.

The higher multipole terms of Equation (7) can also be written in the tensor form of Equation (8) which separates the direction of the field point from the surface integrals.

In the subsequent analysis, we treat $\underline{s}$ as the Lagrangian coordinate of a material point of the wetted surface of the imploding body. This does not invalidate the Kirchhoff equation provided the surface does not change appreciably during the time interval for a sound wave to transit across the body, i.e., provided $\dot{s} \ll c$. Under this same condition, it does not affect the Taylor expansion coefficient given by Equation (5), for

$$t^* - t_o^* = [t - R(t^*)/c] - [t - r(t_o^*)/c]$$

$$= \frac{r(t_o^*) - R(t_o^*)}{c} + \frac{R(t_o^*) - R(t^*)}{c}$$

$$\simeq \frac{a}{c} \cos(\underline{a},\underline{r}) + (t^* - t_o^*) \frac{b}{c} \cos(\underline{b},\underline{r})$$

$$\therefore \quad t^* - t_o^* = \frac{a}{c} \cos(\underline{a},\underline{r}) \left[1 - \frac{b}{c} \cos(\underline{b},\underline{r})\right]^{-1}$$

$$\simeq \frac{a}{c} \cos(\underline{a},\underline{r}) \qquad (9)$$

In practical cases of implosion, we can generally expect the monopole radiation to dominate; our experience indicates that an implosion is accompanied by some "crushing," i.e., some volume change, and Equation (7) shows that a monopole source is the most efficient multipole sound source because of the c^{-m} factor. However, there is no absolute necessity for the higher multipole terms to be negligible, and indeed it is simple to invent situations where the dominant contribution would be from some higher multipole. But the external pressures that initiate the implosion are the same in all directions. The implosion can generate sound pressures with a higher multipole symmetry only if the internal forces and the motions of the wetted surface have this same symmetry.

THEORY OF A SIMPLIFIED IMPLOSION DEVICE

The implosion device which is used in the experiments can be idealized for analysis purposes in the simple schematic form of Figure 1.

Initially, the piston is retained at the top of the air chamber where it seals off the internal air at atmospheric pressure from the

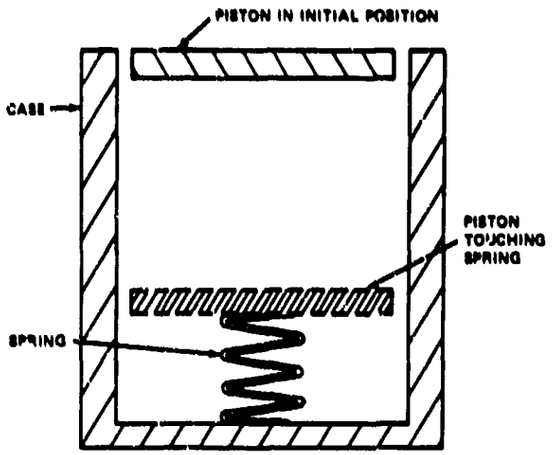

Figure 1 – Idealized Implosion Device

external water at some higher hydrostatic pressure. The piston is then released at some preselected external pressure and is driven down the chamber by the water pressure with increasing velocity until the motion is arrested by impact with the spring or by the pressure of the trapped air. The sharp deceleration, or impact, results in high accelerations of the wetted surface and in a significant production of sound.

To analyze this motion, we assume that the periods of any elastic vibrations of the piston and the case are all very much smaller than the time intervals in which the motions of the piston and case change appreciably. This means that we can treat the piston and case as rigid bodies. We also assume that the transit time of a sound wave in the water across the case is very much smaller than the time interval for the motion to change appreciably. This means that the unsteady pressure distribution in the water adjacent to the piston and case is the same as though the water were incompressible, i.e., the same as though the water acted as an added inertia whose magnitude depended only on the patterns of motion of the piston and the case.

Thus, if $A_1 = \pi a_1^2$ and $A_2 = \pi a_2^2$ are the section areas of piston and case, respectively, and if $x_1(t)$ and $x_2(t)$ are the upward displacements, then the kinetic energy of the water can be written in the form

$$T = \frac{L_1 \dot{x}_1^2}{2} + \frac{L_2 \dot{x}_2^2}{2} \tag{10}$$

where the added water mass due to piston motion is

$$L_1 = 2\rho a_1^3 + \rho A_1 (x_2 - x_1) \tag{11}$$

The first term is the added mass for a thin disk of radius a when one face moves with uniform velocity and the other face is stationary.[3] It thus approximates the added mass of a semi-infinite cylinder moving end-on. The second term is the mass of water in the tube. To the same approximation, the added water mass due to the motion of the case is

$$L_2 = 2\rho a_2^3 \tag{12}$$

These assumptions also imply that the upward force on the water due to the motion of the piston is (from Lagrange's Equation)

$$Q_1 = \frac{d}{dt} \frac{\partial T}{\partial \dot{x}_1} - \frac{\partial T}{\partial x_1} \tag{13}$$

$$= L_1 \ddot{x}_1 + \dot{L}_1 \dot{x}_1 + \frac{\rho A_1 \dot{x}_1^2}{2} \tag{14}$$

$$= L_1 \ddot{x}_1 + \rho A_1 \dot{x}_1 \dot{x}_2 - \frac{\rho A_1 \dot{x}_1^2}{2} \tag{15}$$

and the upward force on the water due to the motion of the case is

$$Q_2 = \frac{d}{dt}\frac{\partial T}{\partial \dot{x}_2} - \frac{\partial T}{\partial x_2} = L_2\ddot{x}_2 - \frac{\rho A_1 \dot{x}_1^2}{2} \tag{16}$$

Note that the force is not simply equal to an added mass times an acceleration. Velocity-dependent terms are present because L_1 varies with x_1 and x_2.

We also ignore sound waves in the air and assume that the air is compressed uniformly and isentropically, so that if P and V are the instantaneous pressure and volume of the air

$$PV^\gamma = P_1V_1^\gamma = P_HV_H^\gamma = P_oV_o^\gamma \tag{17}$$

where P_1 and V_1 are the initial values, P_H and V_H are the values that obtain when the internal pressure is equal to the external hydrostatic pressure, P_o and V_o are the values that obtain when the piston first touches the spring, and $\gamma = 1.4$.

The "spring" is a simple energy-absorbing device whose behavior approximates an ideal linear plastic material. By ideally linear we mean that if W(y) is the work done in dynamically compressing the spring through a distance y (where $\dot{y} = \dot{x}_2 - \dot{x}_1$), then the resisting force is

$$F_s = \frac{\partial W}{\partial y} = ky \tag{18}$$

where the stiffness $k = \partial^2 W/\partial y^2$ is a constant independent of y and independent of the rate $\dot{y}$. By ideally plastic we mean that this work is done irreversibly so that if the compressive force were relaxed, the compres-

sion y would not change. In practice, the "spring" is neither perfectly linear nor perfectly plastic, but these imperfections have minor effects which can be analyzed as perturbations. We pre-position the spring so that contact with the piston first occurs when $V_o \simeq V_H$ and $P_o \simeq P_H$, and pick a spring whose stiffness k is much greater than the equivalent stiffness of the air at this point. In this way the impact energy is near a maximum, the stopping distance is very much shorter than the travel distance $(V_1 - V_o)/A$, and the spring force is the dominant force in the system.

With these approximations, the equations of motion for the piston and case, respectively, are

$$M_1\ddot{x}_1 = (P - P_H)A_1 + F_s - Q_1 \tag{19}$$

$$M_2\ddot{x}_2 = -(P - P_H)A_1 - F_s - Q_2 \tag{20}$$

where M_1 and M_2 are the masses of piston and case, respectively. The first term on the right is the force due to the pressure difference between the air inside and the water outside; the second term is the resistance of the spring and is present only when the piston is touching the spring and compressing it, i.e., only when $V < V_o$ and $\dot{V} < 0$; the last terms are the reactions on the piston and on the case of the unsteady forces in the water. If we substitute for Q_1 and Q_2 the values given by Equations (14) and (16), we have the equations of motion in a more explicit form

$$\frac{d}{dt}\left[(M_1 + L_1)\dot{x}_1\right] = (P - P_H)A_1 + F_s - \frac{\rho A_1 \dot{x}_1^2}{2} \tag{21}$$

$$\frac{d}{dt}\left[(M_2 + L_2)\dot{x}_2\right] = -(P - P_H)A_1 - F_s + \frac{\rho A_1 \dot{x}_1^2}{2} \tag{22}$$

From these we can obtain an expression for the conservation of linear momentum

$$\frac{d}{dt}\left[(M_1 + L_1)\dot{x}_1 + (M_2 + L_2)\dot{x}_2\right] = 0 \tag{23}$$

Or, since $\dot{x}_1 = \dot{x}_2 = 0$ at $t = 0$, then for all t

$$(M_1 + L_1)\dot{x}_1 + (M_2 + L_2)\dot{x}_2 = 0 \tag{24}$$

and this relation is valid whatever the form of the internal forces. There is also a geometrical constraint

$$\dot{V} = A_1(\dot{x}_1 - \dot{x}_2) \ . \tag{25}$$

Equations (11), (12), (17), (18), (21), (22), and (25) are sufficient to completely determine the motions $x_1(t)$ and $x_2(t)$ for any prescribed set of parameters and any initial conditions. The equations can always be solved on a computer by conventional numerical techniques to any desired accuracy. Furthermore, $x_1(t)$ and $x_2(t)$ together with Equations (7) or (8) completely determine the magnitudes of the radiation multipoles and thus completely determine the sound field.

Thus the monopole source strength is

$$\dot{V} = A_1(\dot{x}_1 - \dot{x}_2) = A_1\dot{x}_1\left(1 + \frac{M_1 + L_1}{M_2 + L_2}\right) = \frac{M_1 + L_1}{M} A_1\dot{x}_1 \tag{26}$$

where the reduced mass M is

$$\frac{1}{M} = \frac{1}{M_1 + L_1} + \frac{1}{M_2 + L_2} \tag{27}$$

Also the volume acceleration is

$$\ddot{V} = \frac{M_1 + L_1}{M} A_1\ddot{x}_1 + \frac{\dot{L}_1\dot{x}_1A_1}{M_2 + L_2}$$

$$= \frac{M_1 + L_1}{M} A_1\left(\ddot{x}_1 - \frac{\rho A_1\dot{x}_1^2}{M_2 + L_2}\right)$$

$$\simeq \frac{M_1 + L_1}{M} A_1\ddot{x}_1 \tag{28}$$

regardless of the nature of the internal forces. The peak values of the second term are ordinarily negligible compared to the first term.

To calculate the dipole radiation we take the origin to be on the longitudinal axis of the piston, at a distance b_1 below the wetted surface of the piston and a distance b_2 above the bottom of the case, and take $\underline{n}_o$ as a unit vector pointing upward. Then the magnitude of the equivalent dipole force is

$$F = \iint \rho\dot{v}(\underline{s}\cdot\underline{n}_o)\, d\sigma - \iint p(\underline{n}\cdot\underline{n}_o)\, d\sigma \tag{29}$$

$$= \rho\ddot{x}_1b_1A_1 + \rho\ddot{x}_2b_2A_2 - Q_1 - Q_2$$

$$= x_1 \left[\rho A_1 b_1 - \rho A_2 b_2 \left(\frac{M_1 + L_1}{M_2 + L_2}\right) - L_1 + L_2 \left(\frac{M_1 + L_1}{M_2 + L_2}\right)\right]$$

$$- \dot{L}_1 \dot{x}_1 \left[1 + \frac{\rho A_2 b_2}{M_2 + L_2} - \frac{L_2}{M_2 + L_2}\right]$$

$$= \ddot{x}_1 (M_1 + L_1) \left[\left(\frac{\rho A_1}{M_1 + L_1} + \frac{\rho A_2}{M_2 + L_2}\right) b_1 - \left(\frac{L_1}{M_1 + L_1} + \frac{L_0 - L_2}{M_2 + L_2}\right)\right]$$

$$- \dot{x}_1^2 \frac{\rho A_1 (M_2 + L_0 - \rho A_2 b_1)\ (M_1 + L_1)}{M(M_2 + L_2)} \qquad (30)$$

where $L_0 = \rho A_2 (b_1 + b_2)$ depends on the fixed distance $b_1 + b_2$ and is independent of the position of the origin b_1.

Thus the amplitude of the dipole radiation depends on b_1 which defines the position of the origin, or reference "centroid." If the added inertia L_1 were independent of the motion (as L_2 is), i.e., if $\dot{L}_1$ were zero, and if the centroid is taken at the point where

$$b_1 = \frac{\dfrac{L_1}{M_1 + L_1} + \dfrac{L_0 - L_2}{M_2 + L_2}}{\dfrac{\rho A_1}{M_1 + L_1} + \dfrac{\rho A_2}{M_2 + L_2}} \qquad (31)$$

then the dipole force F would be identically zero (over the duration of the sound pulse) and there would be no far-field dipole ratiation relative to this centroid. Since, in fact, $\dot{L}_1$ is not identically zero, there is some dipole radiation centered at this centroid. But the amplitude of the equivalent dipole sound pressure source is of the order of $\dot{F} = \frac{d}{dt}(\rho A_1 x_1^2)$

which is ordinarily completely negligible compared to the amplitude of the monopole radiation. Note that if $M_1 = M_2$, $L_1 = L_2$, $A_1 = A_2$, then $b_1 = b_2$ which means that the entroid of Equation (31) is halfway between the top of the piston and the bottom of the case. Also if $M_2 + L_2 \gg M_1 + L_1$, as actually occurs, then $b_1 \approx L_1/\rho A_1$ and is independent of b_2.

In a similar manner we can show that the quadrupole radiation is negligible for this simplified implosion mechanism because the external and internal forces which generate the surface accelerations have no net component with quadrupole symmetry.

We can estimate the principal features of the sound radiation quite simply if we neglect the force $(P - P_H)A_1$ in Equations (19) and (20) in comparison with the spring force F_s. Then the equation of motion during impact simplifies to

$$M\ddot{y} + ky = -\frac{\rho}{2}A_1\dot{y}^2\left(\frac{M}{M_1 + L_1}\right)^2 \tag{32}$$

where y is the compression of the spring of Equation (18) and M is the reduced mass. The maximum value of the term on the right is negligible compared to the maximum value of the spring force ky and will be ignored. The initial conditions are that $y = 0$, $\dot{y} = \omega y_m$ where $\omega^2 = k/M$ and y_m is the maximum compression calculated below in Equation (36). Hence the solution for $\dot{y}$ is a quarter sine wave

$$\dot{y} = \omega^2 y_m \sin \omega t \qquad t \leq \pi/2\omega$$

$$\dot{y} = 0 \qquad t > \pi/2\omega \tag{33}$$

and the monopole sound radiation is simply

$$p(\underline{r},t) = \frac{\partial V}{4\pi r} = -\frac{\rho A_1}{4\pi r} V(t_o^*) \approx \frac{\rho A_1}{4\pi r} \frac{M_1 + L_1}{M} \ddot{x}_1 \qquad (34)$$

where the origin is located a distance b_1 below the piston, as given by Equation (31).

We must expect that the necessary deviations of any actual structure from this highly simplified model will have some appreciable effects. These will be discussed when we describe the actual implosion structure.

We also derive a simple estimate of the maximum compression of the plastic spring. Assume that at the time of maximum compression all parts of the system are instantaneously at rest and there have been no energy losses. Then $W(y_m)$, the work done in compressing the spring, must equal the work done by the hydrostatic pressure less the change in the internal energy of the air, i.e.,

$$W(y_m) = P_H(V_1 \quad V_o) - \frac{P_oV_o - P_1V_1}{\gamma - 1}$$

$$= \left[\frac{P_H}{P_1}\left(1 - \frac{V_o}{V_1}\right) - \frac{1}{\gamma - 1}\left(\frac{V_1}{V_o}\right)^{\gamma-1} + \frac{1}{\gamma - 1}\right] P_1V_1 \qquad (35)$$

Thus, if $W(y)$ is known independently and whatever its form may be, then y_m is determined by the initial parameters P_H and V_o. If, in addition, we specify that the spring is linear, then

$$y_{max}^2 = \frac{2P_1V_1}{k}\left[\frac{P_H}{P_1}\left(1 - \frac{V_o}{V_1}\right) - \frac{1}{\gamma - 1}\left(\frac{V_1}{V_o}\right)^{\gamma-1} + \frac{1}{\gamma - 1}\right] \qquad (36)$$

Note that these relations are independent of the masses and the added masses.

EXPERIMENTAL VERIFICATION OF THE THEORETICAL ANALYSIS

EXPERIMENTAL DESIGN

The implosion device used in the experiments was designed to fit the simplified theory and to be usable at depths up to 1000 ft (500 psi over pressure). The construction is shown in Figures 2 and 3. The piston and case were made of stainless steel and weighed about 62 lb in air.

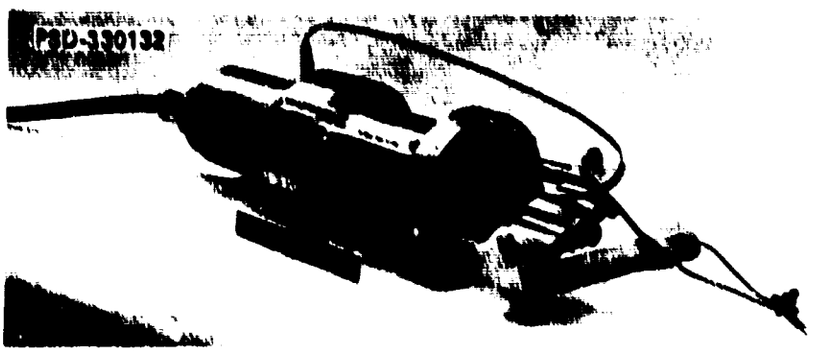

Figure 2 – Implosion Device Ready for Test

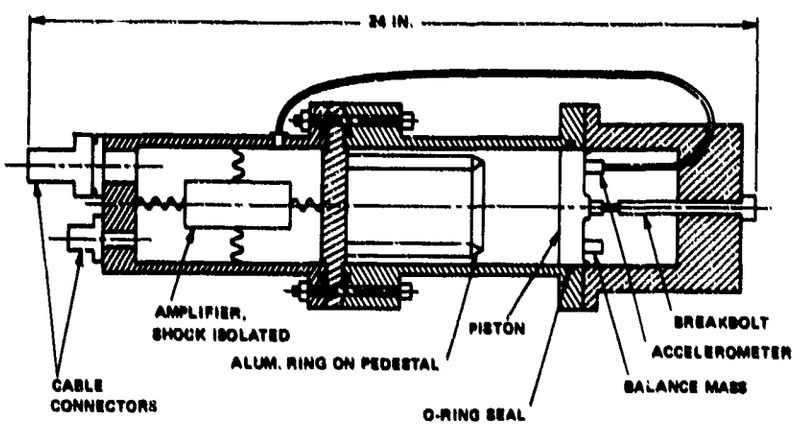

Figure 3 – Schematic Drawing of Implosion Device

The upper chamber in which the piston moved had a bore diameter of 4.01 in., a length of 6.7 in., and a wall thickness of 0.31 in. The upper chamber was initially closed at the top by the piston with an O-ring seal. The lower chamber contained preamplifiers for the instruments.

The "breakbolt" which held the piston in its initial position was screwed to the piston at the bottom and passed through a hole in the narrow "bridge" above. This breakbolt, shown in Figure 4, was made from a stock high-strength bolt, 1/2 in. in diameter and 6 in. long. It was necked down over a 1/2-in. length to a diameter which was calculated to break suddenly when the outside water pressure reached some preselected value. Preliminary tests of these breakbolts showed that the effective tensile strength was 173 kpsi $\pm$ 5 percent and that the elongation before break was less than 0.04 in.

The piston shown in Figure 5 had a diameter of 4.00 in. and was 1.2 in. thick at the edge. The thickness must be larger than the maximum elongation of the breakbolt plus the contact width of the O-ring. Also a greater thickness minimizes the possible tilt in the piston as it travels down the tube, and also increases the frequency of the lowest elastic resonance mode. The piston was honeycombed by drill holes in order to decrease the mass without a proportional decrease in the stiffness. Some auxiliary experiments showed that the lowest elastic resonance mode of the piston had a frequency of about 11.9 kHz and an umbrella-like vibration pattern with a nodal circle whose diameter was 2.59 in.

The impact "spring" was actually a ring of aluminum (shown in Figure 4) which was annealed dead soft to make it plastic; it was given a triangular cross section to make it have an approximately linear response, i.e., to make the force resisting compression approximately proportional

PSD-330134

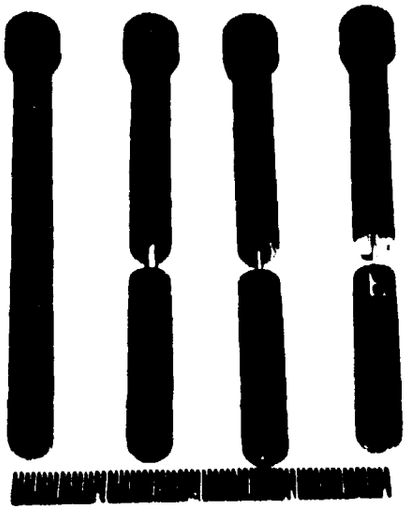

PSD-330135

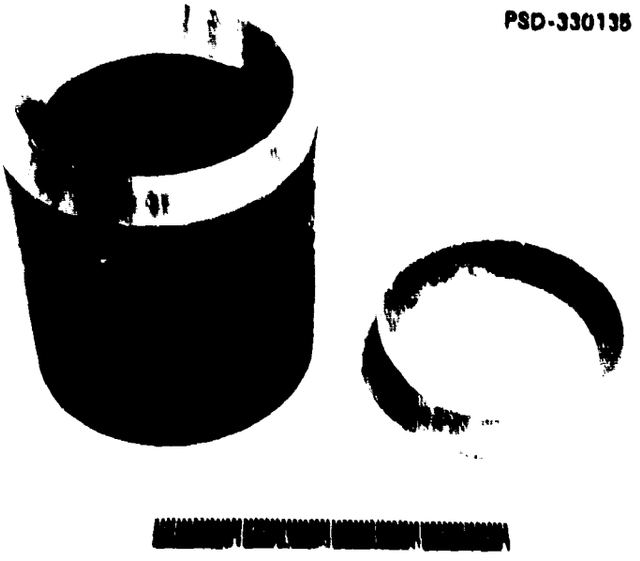

Figure 4 – Breakbolts and Aluminum Rings

PSD-330133

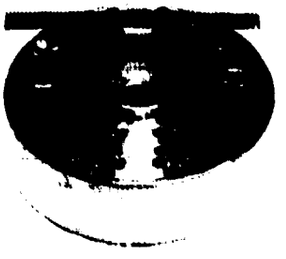

Figure 5 – Piston with Accelerometer and Balance Weight

to the amount of compression. The design of this plastic spring was suggested by experience with crusher gages using soft copper balls.[4,5] The diameter of the impact circle of the aluminum for the early tests was 3.0 in. (In the remaining tests, however, it will be made equal to the diameter of the nodal circle of the vibration pattern of the piston so that impact will not excite the fundamental vibration mode of the piston.)

The cross section of the aluminum ring was in the shape of an isosceles triangle with a base of 0.50 in. and a height of 0.50 in. This shape was chosen because auxiliary tests (described in Appendix A) showed that it had a reasonably linear response with an acceptable equivalent stiffness of $k = 3.98 \times 10^6$ lb/in. (for the 3.0-in. diameter). The aluminum ring was cemented to a pedestal cylinder whose length was selected to place the impact at any desired point along the chamber.

An accelerometer was fastened to the top of the piston at a point above the nodal vibration circle in order to measure the gross vertical motion of the piston and yet be insensitive to any motion in the fundamental elastic mode. (The remaining tests will use two identical accelerometers electrically connected in parallel and placed 180 deg apart on the nodal circle in order to better average the motion over the face of the piston.) The accelerometer was a piezoelectric quartz-crystal device (Kistler Type 805A) with a nominal capacity of 60 pF, a charge sensitivity of 0.283 pC per g, a linear output range up to 10^5 g, and a nominal flat frequency response to above 30 kHz. The accelerometer was connected by 2.5 ft of lo-noise coaxial cable (μ Dot 50-3084) to a preamplifier (Ithaco Type 150 M102) with a nominal input impedance of 10^9 Ω, an output impedance of 50 Ω, and a nominal gain of unity. A small capacitor, which brought the total input capacitance to 286 pF was placed across the preamplifier input in order to attenuate the expected signal below the peak linear range (3.8 V) of the preamplifier. The accelerometer case was attached to the piston by cementing it through a 1-mil-thick fiberglass base with Eastman 910 epoxy adhesive; it was further insulated from the piston and the water by a coating of PRC waterproofing compound. This was

necessary because the accelerometer output lead is electrically grounded to its case.

The hydrophones used to measure the sound pressure (Atlantic Research Type LC32) are made of three cylinders of lead zirconate-titanate each 1/4 in. long by 1/2 in. diameter. They have a mechanical resonance frequency of about 70 kHz, a capacity of about 15,000 pF, and a nominal flat frequency response to about 20 kHz. They were connected by 3 ft of lo-noise cable to a preamplifier similar to that used for the accelerometer (except that it had a gain of five). They were waterproofed by molding hydrophone and preamplifier in polyurethane as shown in Figure 6. The sensitivities of the hydrophone and preamplifier combinations were determined as described in Appendix B; they ranged from 10 to 40 μV/μbar.

A block diagram of the entire instrumentation is shown in Figure 7. The output leads of the preamplifiers were each fed through a long cable (typically Navy Type TTRS-4) to a central junction box. The cable also had one pair of leads for the d-c power to the preamplifiers and another

PSD-330138

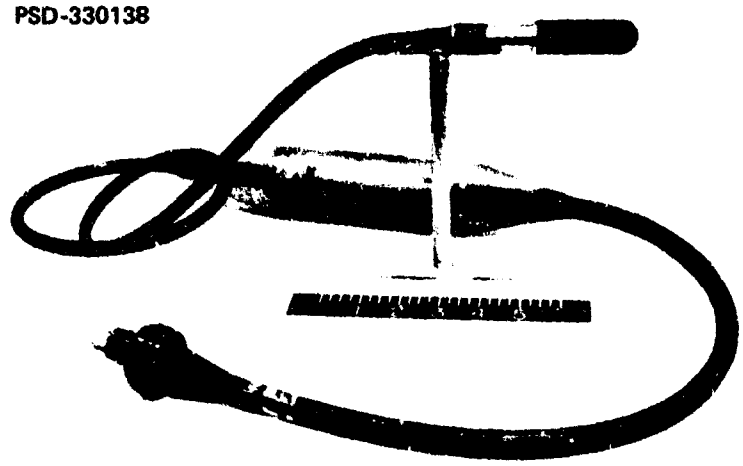

Figure 6 – Hydrophone and Preamplifier

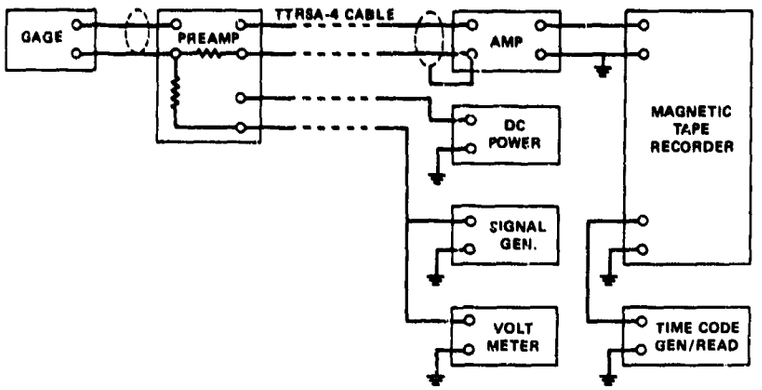

Figure 7 – Block Diagram of Instrumentation

pair of leads for applying a voltage calibration to the input circuit of each preamplifier. The signal from each preamplifier was then amplified by an Ithaco Model 252 amplifier whose input resistance had been shunted to about 50 Ω in order to match the characteristic impedance of the long cable. The signals were then recorded with a tape recorder (Ampex Model FR-1300) operating in an FM mode with a tape speed of 60 ips and an upper frequency response limit of about 20 kHz. A precision 1-kHz timing signal, with the amplitude coded by a time code generator, was simultaneously recorded on one channel of the tape recorder.

After the signals are recorded, they can be visually examined in two different ways. Individual transient pulses can be examined by playing back one channel of the tape through a CRO and triggering the sweep of the CRO by the amplitude of the transient signal. Or all channels of a tape record can be played back simultaneously through a multichannel galvanometer-oscillograph, e.g., Midwestern Model 801 Visicorder, running at paper speeds up to 64 ips. The available galvonometers have a flat frequency response to about 5 kHz. However, if the magnetic tape is

played back at 7.5 ips instead of at the recording speed of 60 ips, the galvanometers can faithfully record input signals to the tape with frequency components greater than the 20-kHz limit of the tape recorder. A single common ground for the entire network was made at the tape recorder. The net frequency response limits of each channel are discussed in Appendix B.

IMPLOSION TEST

The experiments were originally designed to be conducted over a range of initial conditions in deep water. However, difficulties in scheduling the facility were such that the only experimental results to date (August 1970) have been obtained in the tank of the Naval Ordnance Laboratory Hydroballistics Facility.[6] This 100-ft-long by 35-ft-wide tank is 100 ft deep, but at the time of the test it was filled to a depth of 60 ft. The imploder was set to release at a depth of 40 ft, and three hydrophones and the imploder were positioned as shown in Figure 8. This arrangement was selected so that (1) a sound pulse of reasonable amplitude and duration would reach each hydrophone, (2) these pulses would not be obscured by echoes from the boundaries of the tank, and (3) comparable measurements could be made on the axis of the imploder and in a direction of 90 deg to this axis.

The three hydrophones were each suspended at their nominal positions by 1/8-in. wire rope, with the hydrophones pointing in a vertical direction. The imploder was slowly lowered from another 1/8-in wire rope at a rate of about 10 ft/min until the breakbolt fractured. The tape recorder was started about 1 min before the expected fracture. Voltage calibrations were imposed on the preamplifiers before and after the test.

After an implosion, the imploder had to be raised in order to replace and position the breakbolt and the aluminum ring.

For the test at a 40-ft depth, the breakbolt diameter was 0.040 in. and the pedestal height was 4.02 in. This pedestal height was estimated to place the aluminum ring at a position where the kinetic energy of the

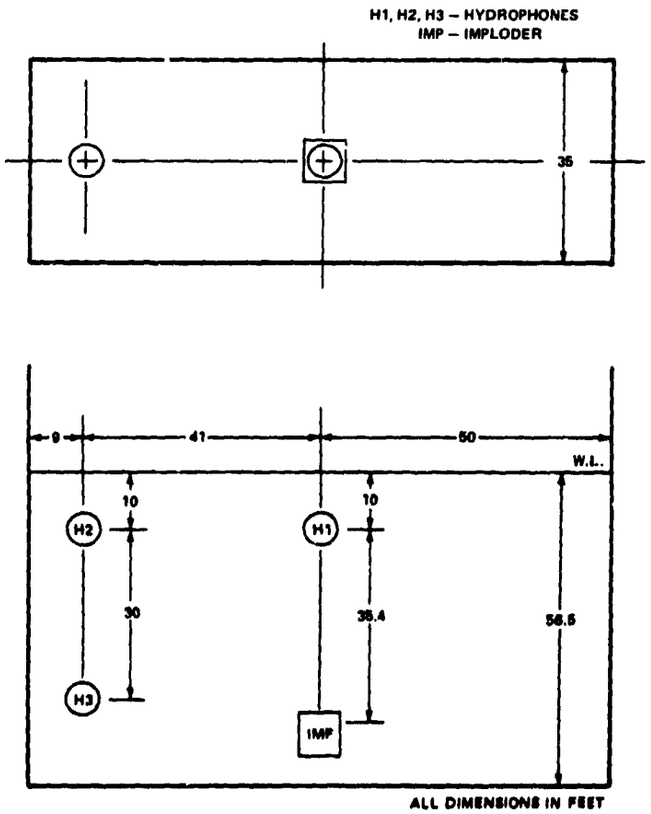

Figure 8 – Location of Imploder and Hydrophones in Tank Test

piston and water would be a maximum. However, it is not critical that these pre-set parameters can be chosen accurately because the actual motion of the piston during impact is measured by the accelerometer.

The other parameters which are necessary for the analysis are listed below. The asterisks indicate quantities that were calculated for the actual impact position.

Spring stiffness	$k = 4.0 \times 10^5$ lb/in
Mass of piston	$M_1 = 1.25$ kg
Mass of case	$M_2 = 26.3$ kg
*Added mass for piston, Equation (11)	$L_1 = 0.90$ kg
Added mass for case, Equation (12)	$L_2 = 3.0$ kg
*Reduced mass, Equation (27)	$M = 2.00$ kg
*Centroid position, Equation (31)	$b_1 = 3.0$ in.
*Depth of centroid at impact	= 44.3 ft
Hydrostatic pressure	$P_H = 2.30$ atm
Initial air pressure	$P_1 = 1.0$ atm
Initial air volume	$V_1 = 65.3$ in^3
Air pressure at impact, Eq. (17)	$P_o = 2.83$ atm
*Air volume at impact	$V_o = 31.1$ in^3

In this test, L_1 and L_2 were uncertain by perhaps 20 and 40 percent, respectively, because the appropriate coefficients in the theoretical equations (Equations (11) and (12)) were likewise uncertain. However, this caused a smaller uncertainty, about 10 percent, in the reduced mass M which affects the amplitudes of the acceleration and sound pressure pulses, an uncertainty of about 5 percent in $M^{\frac{1}{2}}$ which affects the duration of the acceleration and sound pressure pulses, and a negligible uncertainty in the ratio $(M_1 + L_1)/M$ in Equation (28).

TEST RESULTS

The test results which are available after an implosion are: (1) a record of the acceleration of the piston versus time, (2) records of the sound pressure versus time at each hydrophone, and (3) a measurement of the set deformation of the aluminum ring.

The measured compression of the aluminum was 32.6 ± 1.0 mils which is about 22 percent below the value of 41.6 mils calculated from Equation (36). The difference is probably due to energy losses as the piston moves down the tube and to the fact that at the time of maximum compression some of the energy must have gone into elastic waves in the structure. In fact, as will be discussed, the accelerometer record can be interpreted to show that there must have been an elastic vibration of the piston with an amplitude of about 10 percent of the plastic displacement. It must also be verified that the assumed spring stiffness, which was measured in calibration tests with high-impact energies is applicable for the small impact energy of this tank test.

The sequence of events can best be verified from Figure 9 which is a Visicorder record of the 1-kHz timing trace and the accelerometer and hydrophone signals. The first signal on the accelerometer record was due to the impact with the aluminum ring. Prior to this, there was no signal above the noise level at the expected time of fracture of the breakbolt, nor any signal which might be due to impact of the moving piston with the side of the case. About 14 msec after the impact signal, there was a sharp pulse of unknown origin; this may have been due to mechanical shock of the preamplifier in the case. The signal record from each hydrophone shows the initial sound pulse direct from the implosion followed by a series of echoes from the top (T), bottom (B), or sides (S) of the tank. Thus H1, H2, and H3 identify the sound pulses direct from the implosion to Hydrophones 1, 2, and 3, respectively; B1, T1, and S1 identify the echo pulses which reach H1 after reflection from the bottom, top, or sides, respectively, etc.

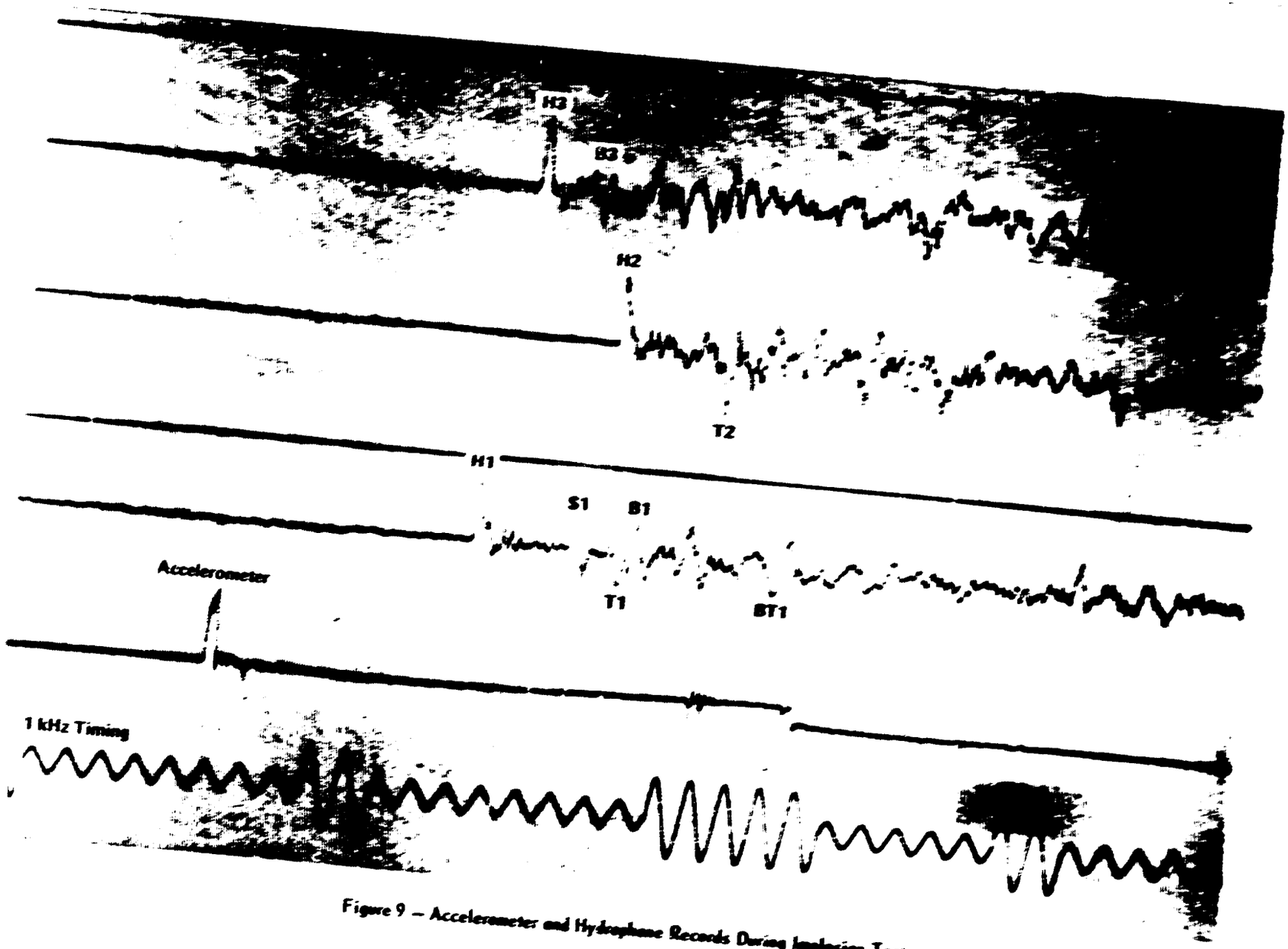

Figure 9 – Accelerometer and Hydrophone Records During Implosion Test

The tabulation given below indicates the path length (as calculated from the geometry of Figure 8) and the travel times (as measured in Figure 9) for each sound pulse identified in Figure 9. We expected that reflection from the top surface would reverse the polarity of the pulse, whereas reflections from the bottom or sides would maintain polarity. However, the apparent echoes from the bottom and sides do not always show the expected polarity (e.g., (B3) pulses) because a sheet of material was hanging vertically in the tank in front of the side wall, and this material could have acted as a soft reflector. Some pulses could not be identified at all. Figure 10 is a plot of path length versus travel time. The data fit a straight line through the origin with a slope of 4830 fps; this is an acceptable value for the speed of sound in city water at a temperature of about 70 F.

Pulse	Path Length, ft	Travel Time, msec
H1	35.4	7.43
S1	49.6	10.27
T1	55.4	11.53
B1	57.6	12.06
BT1	77.6	15.93
H2	53.8	11.15
S2	64.2	?
S2	68.8	?
T2	68.9	14.29
B2	70.6	?
H3	41.4	8.42
B3	50.3	10.75
S3	54.4	?
S3	59.1	?

We shall analyse the direct pulses further; however, too little is known about the nature of the reflection coefficient from each surface to make it profitable to examine the echoes. In fact, the echoes might be analysed to estimate the magnitudes of the reflection coefficients.

Figure 11 shows the accelerometer signal with an acceleration scale determined from the voltage calibration and a time scale determined from the timing trace. The dashed line curve is the theoretical curve

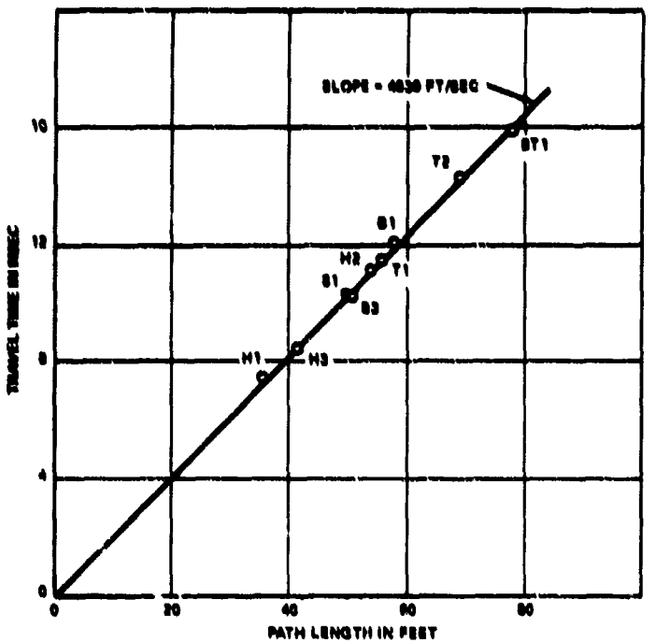

Figure 10 – Path Length versus Travel Time for Hydrophone Pulses

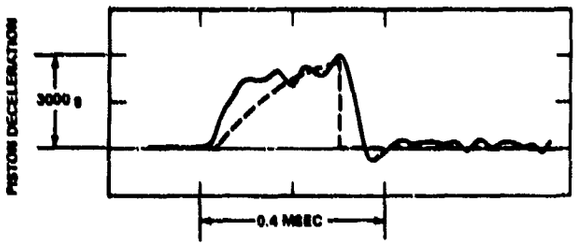

Figure 11 – Piston Acceleration versus Time

$$\ddot{x}_1 = \frac{M}{M_1 + L_1} \omega^2 y_m \sin \omega t \; ; \; \omega^2 = k/M; \; t \leq \pi/2\omega \qquad (37)$$

with y_m taken as its measured value (32.6 mils). This curve has been drawn to the same scales as the measured acceleration and is arbitrarily placed so that the peak accelerations occur at the same time. The two curves are grossly similar. However, the peak measured acceleration was about 6 percent above the theoretical peak, the duration of the measured pulse was about 0.34 msec compared with 0.26 msec for the theoretical curve, and the measured acceleration had an oscillation at about 15 to 20 kHz superimposed on the mean pulse. These differences could all be due to two effects which have been ignored in the simplified theory: (1) the piston might be tilted as it moves down the tube and hit the aluminum spring nonuniformly and (2) there are undoubtedly elastic modes of the piston and case with periods which are not very small compared to the duration of the pulse, and we cannot ignore them by analyzing the piston and case as rigid bodies.

Since the diameter of the cylinder bore was about 30 mils more than the diameter of the piston, then at the time of first impact with the spring the center of the piston could be above the spring by as much as

$$d = \frac{\text{radius of spring}}{\text{edge thickness of piston}} \times 30 = \frac{1.5}{1.1} \times 30 \approx 40 \text{ mils}$$

The impact must then rotate and straighten the piston, as well as decelerate it. The duration of the acceleration pulse will be increased, but pending a more detailed analysis, it is not certain what effect this will have on the amplitude or shape of the acceleration curve at a single accelerometer. Perhaps the fact that the measured compression of the alu-

minum was fairly uniform around the rim is some indication that the peak deformation and peak acceleration are not greatly affected, and perhaps this explains why the peak values of the two curves in Figure 11 agree as well as they do.

There are several elastic modes which could explain the oscillations on the accelerometer record. There must be a longitudinal vibration of the spring pedestal with a frequency in the range 15 to 25 kHz. There is a flexural mode of the piston with a frequency about 12 kHz. There could easily be elastic modes in the case with frequencies in this range. The comparatively slow drop in the acceleration from its peak value and the negative peak of about 10 percent of the positive peak must be due to some kind of elastic motion.

We next compare the signals from the three hydrophones. For this purpose they are shown superimposed in Figure 12. The time scale has been shifted so that the peaks approximately coincide in time, and the pressure scale has been magnified in direct proportion to the travel distance from implosion to hydrophone. The numerical value on the vertical scale can be interpreted as the sound pressure which would be measured at the same angular direction but at a common range of 100 ft.

There was good agreement, on the order of 15 percent, between the three records for the first 0.3 msec which covered the development and decay of the principal pulse. After 0.3 msec, the signals were smaller and differed appreciably; the H1 hydrophone (on the longitudinal axis) showed the most complex signal and the H3 gage (at 90 deg to the axis) showed the simplest signal. This makes it plausible that a monopole source dominated in the first 0.3-msec period, whereas a longitudinal dipole or longitudinal quadrupole source dominated at later times. This

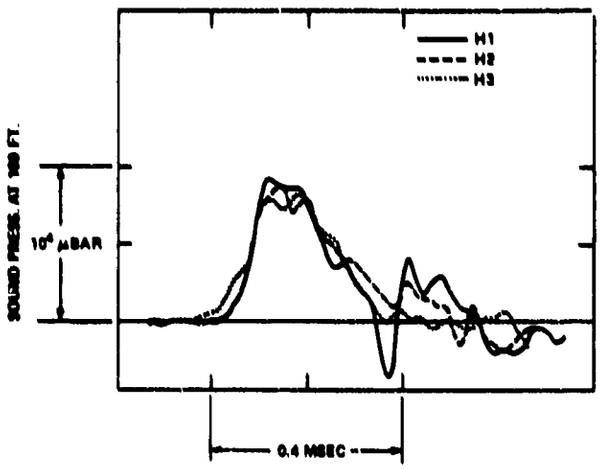

Figure 12 – Comparison of the Three Hydrophone Records Adjusted to a Common Range

is in accord with the previous discussion of the acceleration pulse because (1) the rigid body rotation of the piston can generate no monopole radiation and negligible higher multipole radiation, (2) the principal source of monopole sound is due to the plastic motion and thus should be complete within 0.3 msec, and (3) the longitudinal elastic motions that persist will radiate as longitudinal dipoles or quadrupoles.

Since the sound pressure off the side should be free of any longitudinal dipole or longitudinal quadrupole component, we compare in Figure 13 the sound pressure at Hydrophone 3 with a theoretical monopole radiation at this range. The latter was calculated from the volume acceleration of Equation (28) with $\ddot{X}_1(t)$ taken as the experimental values of Figure 11. Note that there was good agreement in the durations of the pulses but that the H3 signal was sharper and about 20 percent higher than the calculated monopole radiation. The deviations would clearly be reduced if we could correct the accelerometer record to measure the mean acceleration over the face of the piston rather than the acceleration at one arbitrary point.

The experimental data are too sparse to justify any quantitative deduction of the magnitudes of the dipole and quadrupole radiation and to explain their dependence on elastic modes in the imploder. Likewise, the

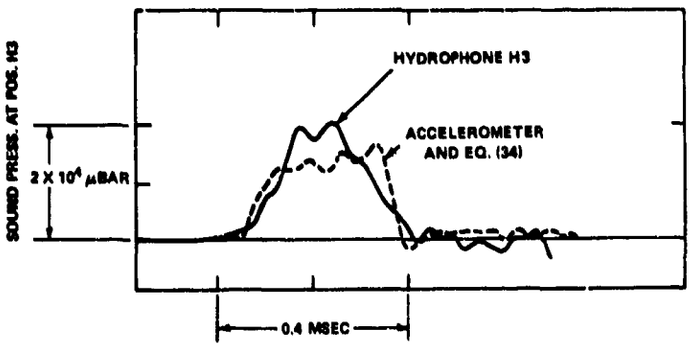

Figure 13 – Comparison of Sound Pressure Measured at Off-Side Hydrophone with Theoretical Monopole Component

data are not sufficient to justify any deduction of the mean motion of the piston or a more precise calculation of the monopole radiation. It should also be added that the hydrophone sensitivities are not known to better than 10 to 15 percent, particularly in the frequency range which is important in these transient pulses. In fact there is some small additional evidence that the hydrophones may appreciably distort sound pulses similar to those in Figure 12, but the data are inconclusive.

SUMMARY AND CONCLUSIONS

1. The general case of sound production by an imploding structure is analyzed into multipole components, where the amplitude of each component depends on a particular average of the acceleration and pressure over the wetted surface of the structure. In most cases, the dominant contribution will be due to the monopole component which is proportional to the second time derivative of the volume enclosed by the wetted surface.

2. In the particular implosion mechanism used in the experiments, the principal sound production is associated with the impact of two parts of the structure rather than with the initial collapse mechanism or with the inrush of water.

3. The theoretical analysis of the impact mechanism and of the generation of monopole sound radiation is substantially verified by the limited experimental data.

4. There are significant variations in the experimentally observed motions and sound pressures from the simplified theoretical analysis. It is plausible that these are due to nonsymmetric impacts and to the presence of low-frequency elastic vibrations in the structure, but the experimental data are too sparse to establish any quantitative relation.

5. For the additional tests planned, the implosion depth will range up to 500 ft, and the sound pressure will be measured at about the same range at points above, below, and off to the side of the implosion. There will be more accurate measurements of the surface-average motion of the piston and more accurate voltage calibrations of each recording channel. The magnitude of the elastic oscillations relative to the plastic motions should be reduced because the support pedestal for the aluminum will be shortened, the piston will be stiffened, and the plastic spring will be softer, thus lengthening the plastic response times versus the elastic response times. It is expected that the new data will resolve the uncertainties in the present analysis.

APPENDIX A

CALIBRATION OF THE ALUMINUM RINGS

The effective dynamic stiffness of the aluminum ring was determined by calibration tests which simulated the behavior of the ring in the implosion.

The ring was placed on a 300-lb steel mass which rested freely on a concrete floor. A 62.4-lb brass weight was dropped from an adjustable height and impacted the aluminum. The falling mass was guided along a 0.5-in.-diameter rod on a nylon bushing. Six drop tests were made with two different sizes of rings. One ring size had a triangular section 1/2 in. wide by 1/2 in. high, and the diameter of the impact circle was 3.0 in. The size of the other ring was the same except for a 1.5-in.-diameter impact circle.

Figure 14 shows the measured values for the mean compression of each ring after impact, versus the height of drop divided by the diameter of the impact circle. The latter coordinate is proportional to the impact energy per unit length of impact, and we can expect this parameter to determine the resultant deformation so long as the initial cross-section shape of the ring was the same in all rings. It is seen that all points had a reasonable fit to the solid line with a slope of 1/2, thus indicating that the final deformation was proportional to the square root of the impact energy. It is true that the data fit the dashed line, with a slope of 0.51, equally well or better. However, the square root relation is within the experimental error and is easier to use in the analysis.

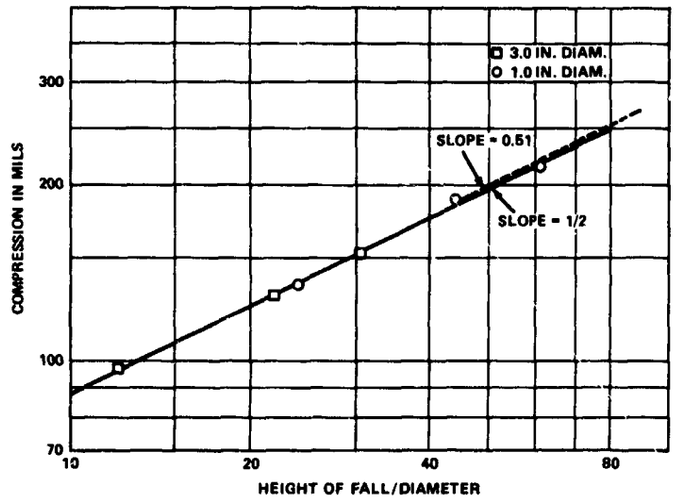

Figure 14 – Calibration of Aluminum Rings

On the basis of this solid line curve and assuming that the bottom mass does not move, the apparent stiffness of the 3.0-in.-diameter ring is

$$k_o = (4.80 \pm .08) \times 10^5 \text{ lb/in.} \tag{A1}$$

However, we can correct this apparent value for the effects due to the finite mass and the probable motion of the bottom. Thus, let M_1 and M_2 be the top and bottom masses, respectively; let u_1 be the impact velocity of the top mass and u_2 be the common velocity of the top and bottom when the deformation of the aluminum reaches its maximum value. Then from the conservation of energy and assuming that the bottom is free to move

$$\frac{M_1 u_1^2}{2} = \frac{M_1 + M_2}{2} u_2^2 + \frac{ky^2}{2} \tag{A2}$$

and from the conservation of momentum

$$M_1 u_1 = (M_1 + M_2)\, u_2 \tag{A3}$$

Hence, we can eliminate u_2 and find

$$k = \frac{M_2}{M_1 + M_2}\left(\frac{M_1 u_1^2}{y^2}\right) = \left(\frac{M_2}{M_1 + M_2}\right) k_o \tag{A4}$$

and for the aluminum ring with a 3.0-in. diameter

$$k = \frac{300}{362.4} \times 4.80 \times 10^6 = 3.98 \times 10^6 \text{ lb/in.} \tag{A5}$$

The proper value for the effective stiffness of the aluminum ring is somewhere between the values given by Equations (A1) and (A5), but for the high frequency motions considered here, we believe that the foundation was effectively soft and that Equation (A5) is the more accurate value.

BLANK

APPENDIX B

SENSITIVITIES AND FREQUENCY RESPONSE CHARACTERISTICS OF TRANSDUCERS AND ELECTRONIC CHANNELS

The sensitivity of the accelerometer was checked only by comparison with a Kestler Model 808K accelerometer which is also a quartz-crystal device. For this purpose the two accelerometers were mounted on a shake table, with the 805A on top of the 808K. The frequency was varied over the range 50 to 1000 Hz, and the signals from the two accelerometers were compared in a simple transfer circuit. The signal amplitudes were found to be in the ratio of the normal sensitivities within about 2 percent. Hence the sensitivity of the 805A accelerometer was taken as 0.283 pC per g. Note that both accelerometers are simple quartz crystal devices which can be expected to have stable and predictable responses except for accidental mechanical damage or accidental electrical leakage to ground.

For these tests it was desirable to have an absolute calibration of the sensitivity of each hydrophone for pulses of the shape shown in Figure 12, which means for frequencies in the range 0.1 to 20 kHz. The calibrations supplied by the manufacturer showed a variation in sensitivity of the order of $\pm$ 1.5 dB over this frequency range. Furthermore, it is likely that the sensitivity at any one frequency in this range is uncertain by 1 or 2 dB. Some attempt was made to obtain an absolute calibration of those hydrophones by using a vibrating column of water.[7] But this method could be used only at low frequencies (up to 400 Hz) and even

then there is no reliable indication of the magnitude of the absolute error. Accordingly, the sensitivities of the three hydrophones were taken as

Hydrophone 1: 7.6 μV/μbar

Hydrophone 2: 37.6 μV/μbar

Hydrophone 3: 38.0 μV/μbar

These are the manufacturers' values for a frequency of about 2 kHz. We expect that these values may be off by as much as 20 percent in absolute value. However, the relative sensitivities of two hydrophones are probably accurate to perhaps 10 percent.

A voltage calibration of any accelerometer or hydrophone channel is best made by imposing a known step voltage (or square wave) to the calibration resistor in the input circuit to the preamplifier, with the transducer connected to the input, and with the amplifier and recorder gains set exactly the same as when recording the signal. Then if R_o is the calibration resistor, R is the calibration resistance plus any lead resistance plus any series resistance in the calibration circuit, C is the gage capacitance plus any lead capacitance plus any terminal capacitance, and V is the applied step voltage across R; the deflection versus time of the recorded calibration signal is exactly the same as though a step acceleration $a_c(t)$ were imposed on the accelerometer, where

$$a_c = \frac{C}{S} \frac{R_o}{R} V \qquad \text{(B1)}$$

and where S is the charge sensitivity of the accelerometer. Furthermore, the rise time and overshoot of the recorded voltage step is a good measure of the upper frequency response limits of the entire amplifier and recorder system, whereas the decay in the recorded voltage step is a good measure of the low-frequency response.

Figure 15 shows the output record of a 10-Hz square-topped wave applied to the input of the accelerometer preamplifier. The output decayed about 23 percent in 50 msec. This implies a decay time of 0.19 sec which is in agreement with an RC of the input circuit equal to $0.67 \times 10^9 \Omega$ times 286 pF. The initial part of the rise, shown on a time-expanded scale, had an overshoot of about 15 percent and a small oscillation at about 30 kHz. Altogether, this voltage calibration showed that a voltage pulse will be recorded with negligible error provided the rise time is more than say 20 μsec, and the decay time is less than 1 msec. The records of Figures 11 and 12 certainly satisfy these criteria.

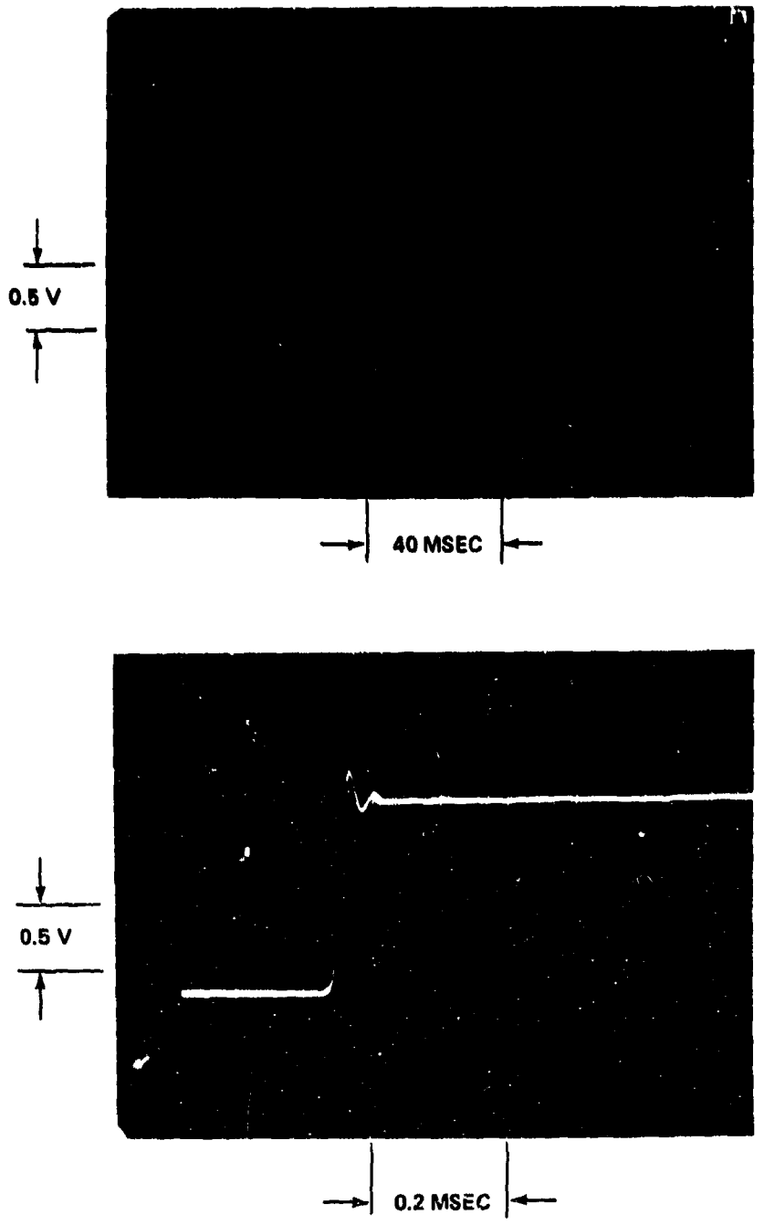

Figure 15 – Voltage Calibration Signals for Acceleration Channel

REFERENCES

1. Baker, B.B. and Copson, E.T., "The Mathematical Theory of Huygen's Principle," Second Edition, Section 5.1, Oxford University Press, London (1950).

2. Morse, P.M. and Ingard, K.U., "Theoretical Acoustics," McGraw Hill Book Company, Inc., New York (1968) pp. 309-314.

3. Rschevkin, S.N., "The Theory of Sound," Chapter XI, Pergammon Press, New York (1963).

4. Abkowitz, D.E., "High-Speed Compression Tests of 3/8-Inch Copper Balls," David Taylor Model Basin Report C-147 (Nov 1948).

5. Chertock, George, "The Response of a Ball Crusher Gage," David Taylor Model Basin Report 751 (Apr 1951).

6. Siegel, A.E., "The Hydroballistics Facility at NOL," Naval Ordnance Laboratory Report NOLTR66-125 (Aug 1966).

7. Schloss, F. and Strasberg, M., "Hydrophone Calibration in a Vibrating Column of Liquid," J. Acoust. Soc. Am., Vol. 34, No. 7 (Jul 1962).